Ultramicroscopy 202 (2019) 121–127

Contents lists available at ScienceDirect

Ultramicroscopy

journal homepage: www.elsevier.com/locate/ultramic

An in-situ approach for preparing atom probe tomography specimens by xenon plasma-focussed ion beam

J.E. Halpin[a,*], R.W.H. Webster[a], H. Gardner[b], M.P. Moody[b], P.A.J. Bagot[b,*], D.A. MacLaren[a]

[a] SUPA, School of Physics and Astronomy, University of Glasgow, Glasgow G12 8QQ, UK
[b] Department of Materials, University of Oxford, Parks Road, Oxford OX1 3PH, UK

ARTICLE INFO

Keywords:
Atom probe tomography
Sample preparation
Focussed ion beam

ABSTRACT

A method for the rapid preparation of atom probe tomography (APT) needles using a xenon plasma-focussed ion beam (FIB) instrument is presented and demonstrated on a test sample of Ti-6Al-4V alloy. The method requires significantly less operator input than the standard lift-out protocol, is site-specific and produces needles with minimal ion-beam damage; electron microscopy indicated the needle's surface amorphised/oxidised region to be less than 2 nm thick. The resulting needles were routinely analysable by APT, confirming the expected microstructure and showing negligible Xe contamination.

1. Introduction

Atom probe tomography (APT) has become an indispensable tool for advanced materials characterization, providing unique nano-scale insights into an ever-expanding range of materials. Aside from advances in laser-pulsing, which have enabled the examination of more fragile, less electrically-conductive specimens, a major improvement to APT methodology has come through the use of focussed ion beam (FIB) instruments for sample preparation, which have greatly improved sample yield and facilitated site-specific analyses [1,2]. FIB methods have enabled precise location selection of the nanometre-sized analysis volumes for APT, and continue to facilitate development of correlative techniques that link APT data to results from a range of complementary electron microscopy methods, including, for example, scanning transmission electron microscopy (STEM) and transmission Kikuchi diffraction (TKD). These have been used to correlate grain boundary orientations with chemistries [3]. Despite these successes, FIB-based methods for APT sample preparation can be involved and user-intensive, particularly for novel classes of materials. The most common procedure, used regardless of material type, is termed the 'lift-out' method, whereby the user selects a region of interest, typically $\sim 30 \times 5$ μm on the surface of the sample. The region is firstly coated in a protective layer to limit beam damage from the procedure. The surrounding material is then milled away using a Ga ion beam before a micromanipulator tool is brought into contact with one end of the cantilever-shape, which must then be carefully extracted. Multiple samples are positioned onto individual posts of a custom-fabricated Si microtip coupon, each isolated from its neighbours and milled to a needle-shape geometry. The entire process can be completed in a few hours for amenable samples, but can take several for more problematic materials. A number of steps in the process are vulnerable to critical problems, which can reduce the yield. Problems include failure to remove sufficient material before attempting to extract the cantilever, mis-handling with the manipulator and poor adhesion of the finished needle to the coupon posts. For the latter, even if the samples appear sufficiently stable, the electric or thermal pulses applied during APT analysis often cause complete sample fracture. While only very limited statistical studies on sample yield have been carried out to date, we have routinely observed in particular materials such as perovskites the failure of samples at this junction. The time-consuming nature of FIB preparation has in many institutions become a bottleneck that limits greater usage of APT. A second problem is ion damage caused by the Ga beam, which is a universal concern, and has complicated the analyses of titanium alloys [4], various steels [5,6] and zirconium alloys [7]. Care must also be taken to avoid inducing additional crystalline phases through heating/implantation under the Ga beam. In addition, the reactivity of Ga can be problematic and materials such as III-V semiconductors [8–10] and aluminium alloys [11] readily react with implanted Ga, modifying the chemistry and causing, for example, embrittlement, that can reduce APT yield. Thus, whilst Ga FIB processing of APT samples offers key advantages over electropolishing methods [12,13], it has fundamental limitations and any improvements in APT specimen preparation would be of significant benefit to the materials science community.

* Corresponding authors.
E-mail address: paul.bagot@materials.ox.ac.uk (P.A.J. Bagot).

https://doi.org/10.1016/j.ultramic.2019.04.005
Received 15 February 2019; Received in revised form 4 April 2019; Accepted 10 April 2019
Available online 12 April 2019

In the present work, we outline a promising approach for APT sample preparation that does not require APT samples to be mounted onto a separate coupon. We mill annular trenches directly into a flat sample to leave a central, free-standing shank with a geometry suitable for APT. Direct fabrication of needles 'in-situ', without a separate mount has been proposed previously [14], along with other strategies that use masking to accelerate preparation times and minimise damage [15,16]. However, such in-situ needle fabrication has in general been limited to the edges of previously-thinned, wedge-shaped samples, because much of the bulk material has already been removed and there is a convenient path for any sputtered material to be removed during FIB milling without re-deposition. In addition, the size of the annular trench required to isolate the APT needle from the electric field of the surrounding sample when biased necessitates high Ga currents and prohibitively long milling times [14]. The performance of conventional Ga FIBs at high milling rates or currents is limited by increasing spot size of the liquid metal ion source (LMIS), which for high beam currents results in severely degraded performance [9]. However, FIB instruments equipped with a Xe plasma source (P-FIB) now deliver high beam currents along with far faster milling rates. The use of such Xe P-FIBs for APT sample preparation has been demonstrated previously [17], with the comparatively larger Xe ions showing a reduced penetration depth and increased sputter yield compared to Ga. TEM studies comparing Xe and Ga-based FIBs have shown a significant reduction, of up to 40%, in amorphous damage in Si using a Xe P-FIB [18]. Furthermore, the chemically inert characteristics of Xe make such P-FIBs suitable for APT needle fabrication from Ga-sensitive materials. With these significant advantages, we show a route to rapidly machine viable APT specimens directly into the sample surface. The technique is site-specific, more adaptable to microstructural features without lift-out limitations, and if the FIB is equipped with analytical techniques such as energy dispersive x-ray spectroscopy, they can be carried out prior to fabrication without need to adjust the stage geometry. Since the technique involves milling without moving the sample, it is well suited to automation, further reducing operator intervention.

2. Materials and methods

A test material of Ti-6Al-4V alloy was chosen for this work, obtained from Alpha Resources Inc. as a 0.1 g cylinder, 3 mm in diameter. This was ground then polished to a surface finish of 0.04μm using colloidal silica. This alloy is extensively used by the aerospace industry and a number of atom probe studies have been undertaken on it and related alloys to examine phase chemistries [19,20], the effects of aging [21,22] and exposure to oxygen [23,24]. Common to many studies where a number of comparative specimens need to be analysed, reducing the specimen preparation time and increasing yield are attractive from the perspective of improving sample throughput.

FIB work was carried out using a Thermo Scientific Helios™ G4 P-FIB UXe DualBeam™ FIB/SEM (Glasgow) that was equipped with a Xe plasma source and separate scanning electron microscopy (SEM) column that enables low-damage imaging of samples during preparation. An overview of the procedure is presented in Fig. 1. Firstly, a 200 nm thick, 20 μm diameter circular Pt pad was deposited by electron-beam induced deposition (EBID) to both protect the Ti during subsequent milling stages and assist with later alignment during fabrication (Fig. 1a)). The stage was then tilted to 52° to orient the surface perpendicular to the incident FIB beam and the manufacturer's automation software (iFAST™ 2016, ThermoFisher Scientific) was used to perform annular mills with decreasing inner and outer radii and decreasing ion-beam current (Fig. 1b–f). Initially, a high ion beam current of 1.3 μA was used to rapidly remove the bulk of the material, with a small defocus applied (Fig. 1b)). To preserve the central material from being eroded by the broad tails of the Xe ion beam, a 50 μm-wide column was retained in the centre of this first annular mill. For some samples, and with the milling current kept at 1.3 μA, a triangular 'tab' was milled at the side of the annulus (Fig. 1c) in order to improve visibility and ease of alignment with respect to the atom probe pulsed laser. The routine then ran through a series of annular mills with carefully selected inner and outer radii at decreasing milling currents (Fig. 1, d–f), resulting in a free-standing pillar with a 5 μm radius. For all annular mills, the scan direction was set as a circular path from outer to inner diameter, ensuring the highest possible milling rates on the exposed edges. The outer diameter of the annular trenches illustrated is ~250 μm, which is large enough to be visible under optical microscopy and to ensure that, when the sample is biased, the electric field at the tip is unaffected by the proximity of the sample's polished surface outside of the milled region. The trench depth is 25 μm and each trench takes of the order of 10s of minutes to mill, the rapidity of which illustrates one of the principal motivations for using P-FIB over Ga ion instruments. Moreover, as the software can work through a designated location map, it is feasible to have unattended fabrication of a number of specimens, as shown by the set produced overnight in Fig. 1 h). Although drift correction was not necessary for the small number of needles prepared here, it could easily be incorporated into longer milling routines. In a FIB-SEM system equipped with analytical capabilities such as electron back-scattered diffraction or energy dispersive x-ray analysis, it is thus feasible to map the surface structure and chemistry of a planar sample, identify specific regions of interest for APT analysis, then leave the automated script to mill the annular trenches about those regions without user intervention.

Below a 5 μm radius, direct observation of the needle is required so that milling and polishing can be stopped when it achieves an appropriate radius. Thus, manual milling was performed using the same methodology as that used to sculpt APT needles on coupons [4]. For the smaller annular mills, the outer radius was fixed and only the inner radii decreased, in order to avoid introduction of any additional sharp peaks on the shank. Finally, the needles were finished with a low-energy polish at 5 kV and then 2 kV. This aspect of the methodology follows the same low-kV/low-energy ion polishing technique that is used to minimise surface amorphous damage in Ga ion FIBs [11]. After polishing, typical tip diameters were less than 50 nm with shank angles around 7°; this taper ensured that a sufficient fraction of the needle, typically a few million ions long, could by analysed by APT under standard conditions.

The entire needle fabrication procedure, including manual polishing, took approximately 180 min per needle and is outlined in Table 1, which can be used as a guide for automated scripts. The guiding principle is to balance the rapid, high-current milling stage with the need to preserve needle microstructure. It is particularly important to assess damage and over-milling caused by the 'tails' of the high-current beam profile, which can extend many μm beyond the nominal milling region and should be measured prior to needle fabrication on a sacrificial area of the sample. We adopted a similar approach to that outlined elsewhere [25], slightly over-focusing the beam to minimise the tail width and make the beam profile less Gaussian for all milling currents > 74 pA. To further minimise tail damage, the inner radius of each annular mill was set to be larger than the measured radius of tail damage for the current used. An unusually thick (200 nm) EBID-Pt pad was also deposited over the region to be formed into APT needles, to act as an effective protective layer against milling damage.

The finished needles were transported to Oxford for APT experiments, carried out on a Cameca LEAP™ 5000X HR system. Once carefully aligned, specimens were analysed using a stage temperature of 50 K, laser pulse energy of 50–120 pJ and at a pulse rate of up to 200 kHz. Data were reconstructed and analysed using the standard IVAS™ 3.8.2 visualization software (Cameca).

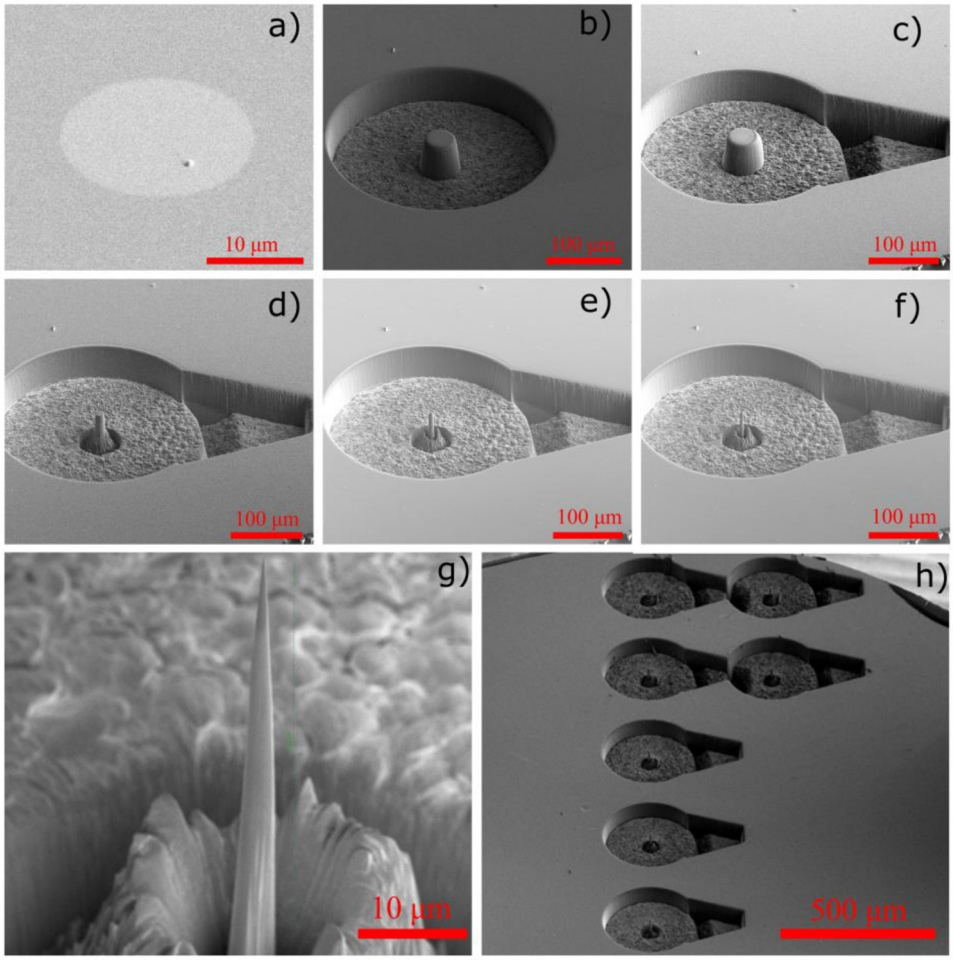

Fig. 1. In-situ fabrication of an array of free-standing atom probe needles. (a) Electron-beam deposited 200 nm-diameter Pt pad; (b) automated 300/50 µm high-current annular mill; (c) automated 'tab' high-current mill; (d) automated 60/15 µm annular mill; (e) automated 18/8 µm annular mill; (f) automated 15/5 µm annular mill; (g) finished needle after manual polishing; (h) automated batch run of 7 APT samples awaiting final manual polishing.

3. Results

3.1. TEM characterisation

To assess the quality of the finished APT specimens, a nano-manipulator was used to lift out a single finished specimen (Fig. 2a)) and transfer it to an Omniprobe® Lift-Out Grid (Fig. 2b)) that had been ion-polished to produce a flat, clean surface for needle mounting. The needle was attached with EBID-Pt and given a final P-FIB polish at 5 and 2 kV in order to remove any damage from the lift-out procedure. To minimise native oxide formation, it was immediately transferred to a JEOL ARM-cFEG transmission electron microscope, with an estimated atmospheric exposure of less than 2 min. A transmission electron microscopy (TEM) image is presented in Fig. 2c), from which the tip diameter was measured to be ~25 nm. The TEM image in Fig. 2d), of the needle shank, clearly indicates a thin amorphous region surrounding the crystalline alloy, the latter marked by the periodic fringes in the image. This region, of either amorphised titanium alloy or of surface oxide, is less than 2 nm thick, which is substantially less than the corresponding region typically observed on Ga ion-prepared needles. This reduced shell thickness is attributed both to the use of a 2 kV polish and the lower damage profiles expected for Xe ions in comparison to Ga ions, as described elsewhere [26]. There were no obvious features associated with beam damage or beam-induced artefacts, such as the formation of Xe bubbles, which have been previously observed by APT [15].

Table 1
Typical needle fabrication work-flow, starting from a flat, polished sample. Note that the times for each step will be material-specific and will differ in accordance with the material's sputtering cross-section.

Application	Voltage (kV)	Current	Shape	(outer/inner) radius (µm)	Depth	Timing (min.)	Notes
E-beam Pt deposit	5	1.4 nA	Circle	20	200 nm	> 20	Automated stage
I-beam mill	30	1.3 µA	Annulus	300/50	25 µm	60	
I-beam mill	30	1.3 µA	Trapezoid	–	25 µm	25	
I-beam mill	30	59, 15, 6.7 nA	Annulus	(60/15), (18/8), (15/5)	25 µm	35	
I-beam mill	30	1.8 nA	Annulus	(12/5), (7/3), (5/2)	10, 10, 10 µm	< 30	Shank profiling
I-beam mill	30	74, 3.8 pA	Annulus	3/ > 0.5	Varied	10	Shank profiling
I-beam mill	(5, 2)	27 pA	Circle	> 0.5	~30 nm	5	Low kV polish

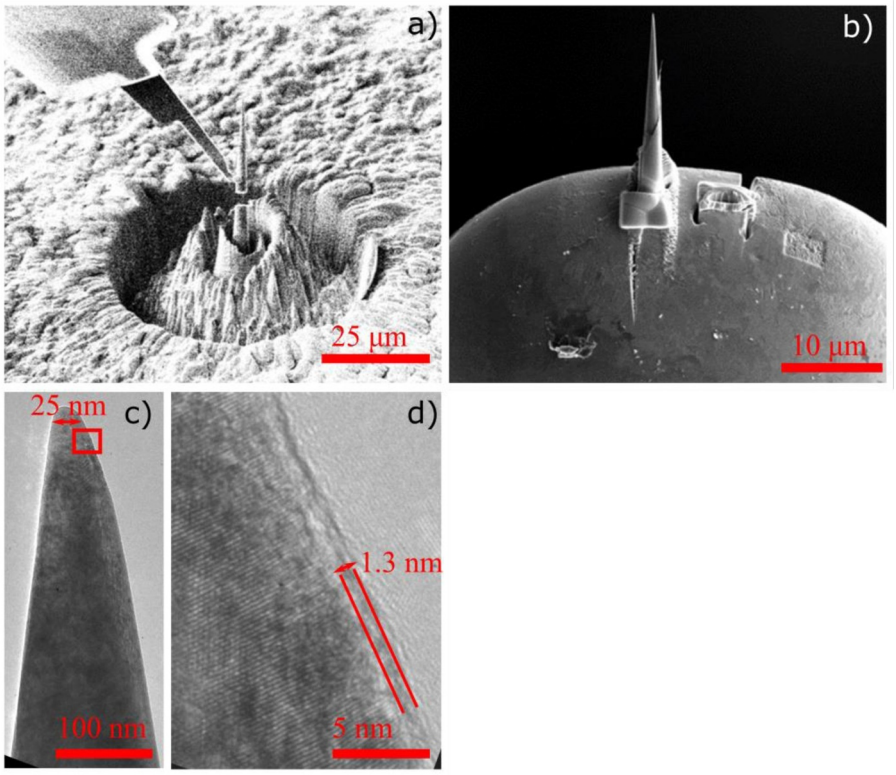

Fig. 2. (a) Quality checking (via lift-out) of a finished APT specimen by nano-manipulator. (b) APT specimen fixed to an Omniprobe® Lift-Out Grid. (c) TEM micrograph showing the profile of a finished specimen. (d) TEM micrograph showing narrow amorphous region at the edge of the needle.

3.2. APT characterisation

The alignment of the Ti-alloy test sample in the analysis stage of the LEAP 5000X HR is shown in side-view in Fig. 3, with the sample lying to the left of each panel and the standard tapered counter-electrode lying to the right. Note the close proximity of the sample surface to the electrode, of the order of 10s of µm, but also the relatively large diameter of the annular milled region in comparison to the counter-electrode. With multiple tips machined into a single planar sample, it was important that the sample surface was flat and mounted as perpendicular to the needle axis as possible, so that the lateral motion required to move between tips did not significantly alter the sample-electrode separation. The close proximity of sample surface and counter-electrode can cause noise from electrode 'turn-on' sooner than would be experienced for a conventional electropolished or lift-out specimen. Care was therefore taken to remove any ragged protrusions or asperities created during ion milling, such as those surrounding the needle in Fig. 2a). A sharp final apex and an electrode that operates noise-free to high voltages is essential to maximise the data obtained. A limitation of the method presented here is that datasets are likely to be shorter than those acquired using more traditional routes, of the order of 10s of millions of ions, because, as the needle becomes progressively blunter, the rising voltage can cause material nearby to generate detector hits.

As outlined above, two different geometries of samples were attempted. The first batch had purely circular trenches, while a second batch had the additional triangular tab to ease the laser alignment in the LEAP. In both cases, the diameter of the milled region exceeds that of the flat face of the counter electrode, so that the electric field is enhanced about the needle apex. In practice, the fully circular geometry was easier to centrally align optically in the LEAP, although for unpolished surfaces the laser-entry tab may be advantageous. When aligned beneath the electrode, the needle tip was readily found by the laser-tip tracking algorithms. Fig. 3 shows selected camera views inside the LEAP when aligning the samples, with (c) showing the laser

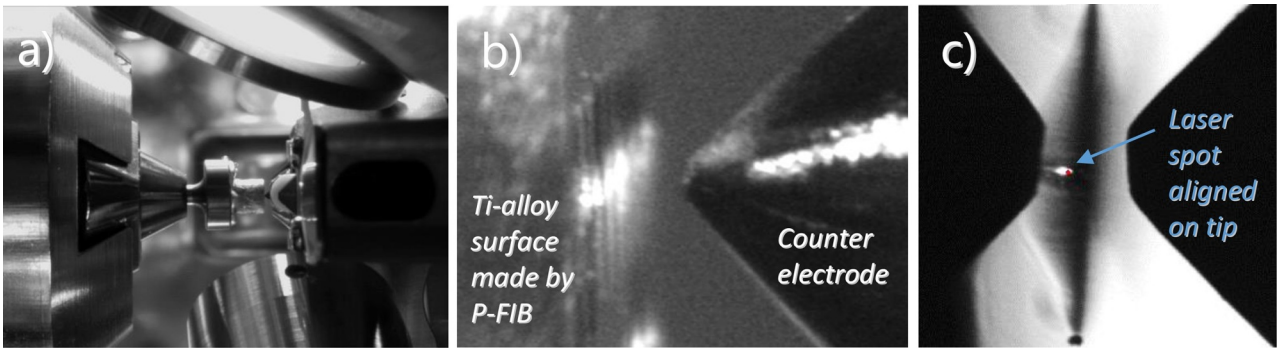

Fig. 3. Ti-6Al-4 V cylinder sample loaded into LEAP 5000X system. (a) Low magnification optical image, showing the sample to the left and the counter electrode to the right. (b) Orientation of moat with the counter electrode. Circumferential cuts in the moat, as viewed from the side, appear as vertical stripes in the sample. (c) A laser-tab moat with the laser focussed on the central needle. (A reflection of the counter-electrode is now also visible on the left of the image.).

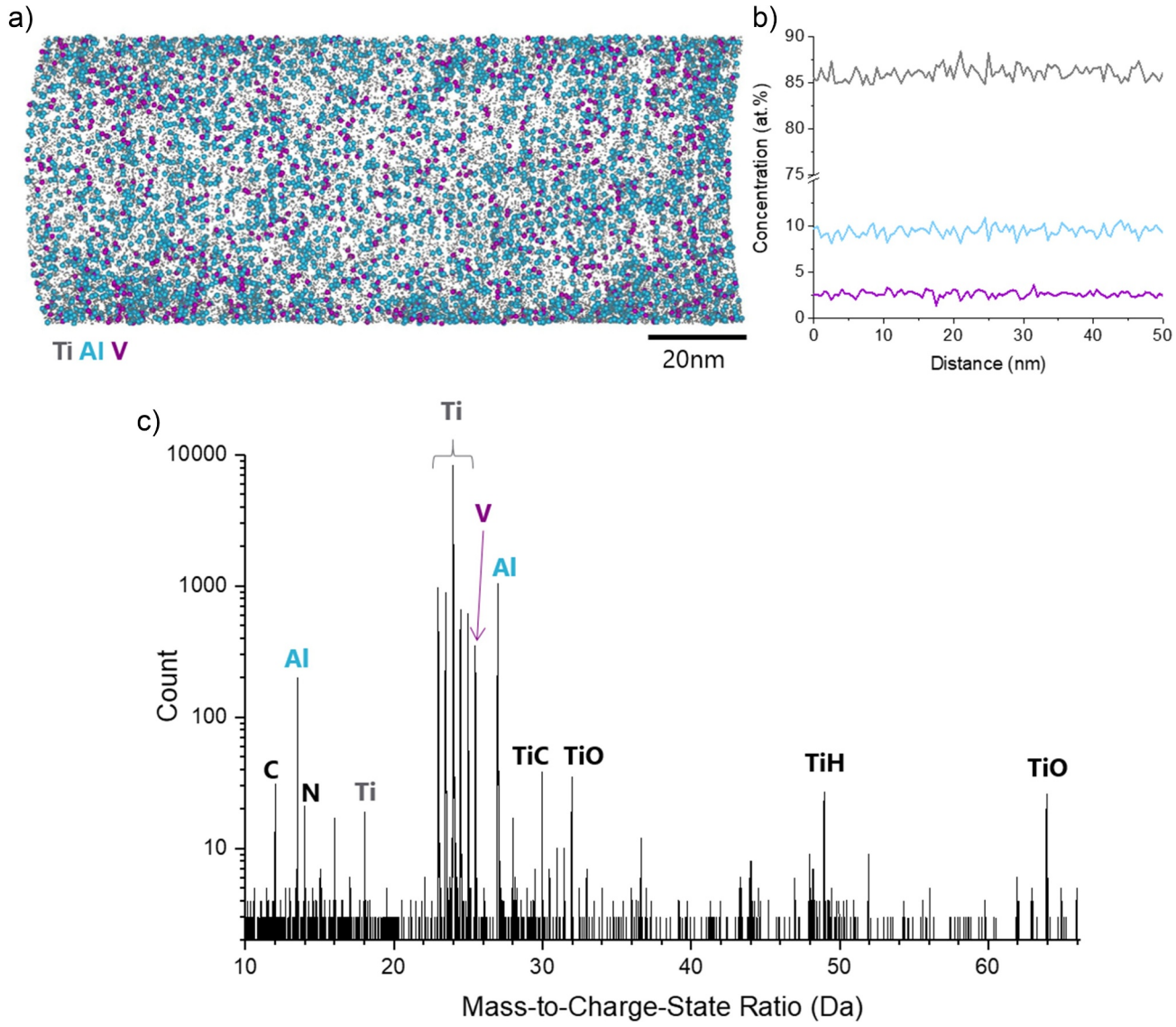

Fig. 4. (a) Atom map of element distributions in Ti-6Al-4V specimen as made by P-FIB (10% of all ions magnified for clarity) (b) 1D concentration profile from same volume as a), highlighting the uniform composition of Ti alpha phase. (c) Mass spectrum of a) with prominent peaks identified (note logarithmic ordinate axis scale).

focussed on the central needle.

Fig. 4 shows a typical acquired mass spectrum (3 M ions) and reconstructed atom map/1D concentration profile to illustrate the viability of the APT data. The mass spectrum is free from any sign of Xe contamination (no peaks were detected in the Xe^{+} range at 124–136 Da as identified in the study by Estivill et al. [17]), and it demonstrates good mass resolution and a high signal-to-noise, indicative of a well-formed, stably-running specimen. The atom map data and 1D concentration profile (reconstructed from the bulk of the dataset) confirm that suitable reconstructions can be obtained, returning a homogenous structure and expected composition for the dominant alpha phase in this Ti-6Al-4V alloy [23]. Turning attention to contaminants, and to allow comparison of this data with those from conventional Ga ion FIBs, Fig. 5 presents a series of 1D concentration profiles from three different Ti-6Al-4V samples, all extracted parallel to the analysis direction and capturing approximately 60 nm depth, including ions from the original outer surface (routinely cropped in normal APT analysis of bulk materials) to highlight relative surface contamination effects. Along with for the P-FIB produced material (solid green line), profiles for V, Ga, C and N species are shown for two Ga ion FIB produced samples labelled 'Control 1′ (orange dotted line) and 'Control 2′ (black dashed line). These specimens of Ti-6Al-4V were produced by the standard lift-out method using a Thermo Scientific Helios and Zeiss NVision respectively. In Fig. 5, the profiles of firstly the minor alloying element vanadium are shown, demonstrating that the P-FIB and 'Control 1′ specimens return a uniform and expected V content of ~2.5 at.% in the dominant alpha phase. For 'Control 2′, the initial stages of the run capture a region of the minor beta phase, illustrated by the high V content, which then falls back in-line with the other specimens when entering the alpha region. Fig. 5 also shows the Ga contaminant profile in 'Control 1′ and 'Control 2′. No corresponding Xe signal was detected in the P-FIB specimen, but it is apparent in both control specimens that Ga ions are embedded throughout the analysed depth, concentrated at the outer surface and to a higher level in 'Control 2′. Note both specimens were prepared using a final 2 kV milling stage aiming to minimise any Ga-damage. Lastly in Fig. 5, the C and N levels are shown for all 3 specimens. It can be seen that aside from a relatively high level of carbon surface contamination in 'Control 2′, which may correlate with the higher Ga level, all 3 specimens show similar and uniformly-low levels of C and N. Overall, the P-FIB preparation produces samples which are at least as contaminant-free as anything made by conventional Ga ion FIBs.

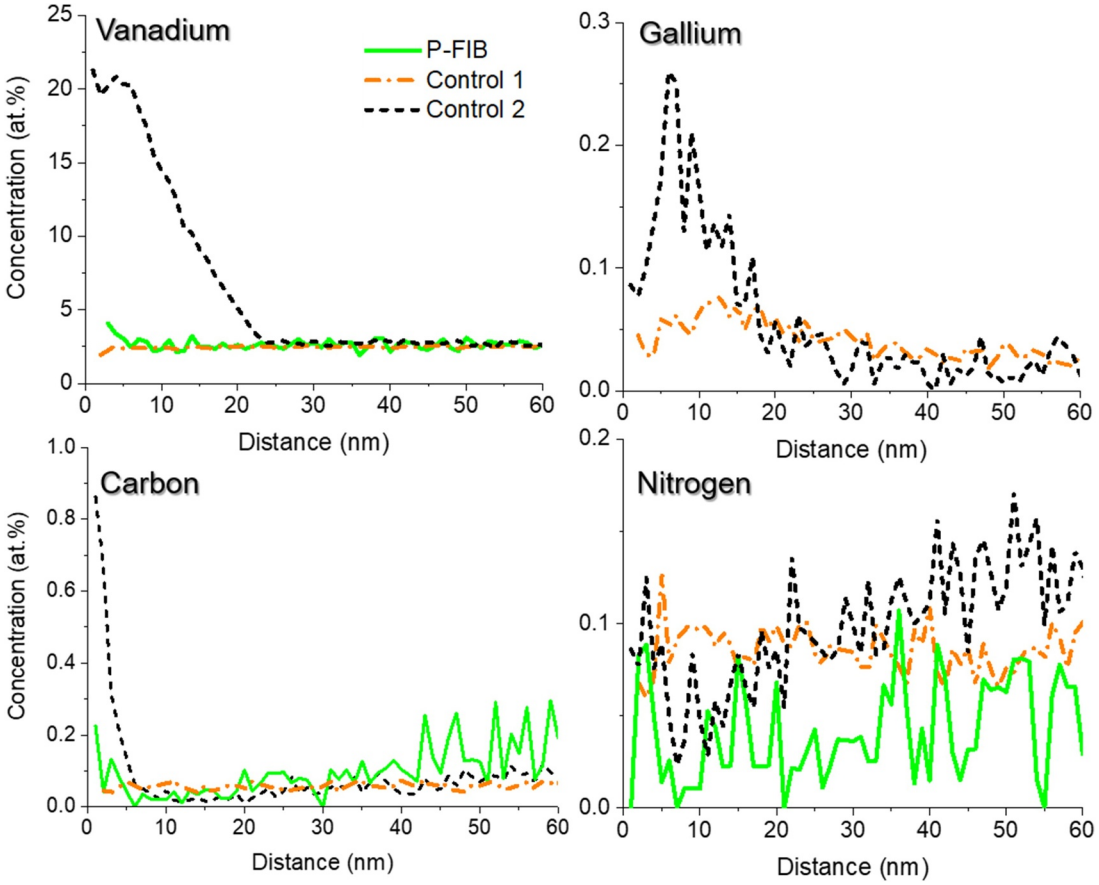

Fig. 5. 1D concentration profiles aligned along specimen axes for Ti-6Al-4V made by P-FIB (green solid lines), Thermo Scientific (Ga) Helios – 'Control 1' (orange dotted lines) and Zeiss (Ga) NVision – 'Control 2' (black dashed line). Profiles show distribution of: Vanadium (sampling beta phase in 'Control 2'), Gallium, Carbon and Nitrogen.

4. Discussion

The APT needle fabrication protocol outlined here offers a fast, in-situ and site-selective method to make multiple APT specimens by Xe P-FIB. A key advantage is that problems and low yields associated with needle lift-out and mounting are avoided. Despite the increase in materials amenable to APT, some classes remain highly challenging to collect even minimal amounts of APT data using conventional needle preparation protocols. In such cases, the attachment of the material to the Si lift-out post (typically a Pt or W FIB-deposited 'weld') is observed by many APT research groups as the likely failure site. In contrast, the in-situ machining approach described here obviates the risk of weak attachment from either poor quality deposition and/or operator error. While yield statistics are difficult to generate without dedicated studies on large numbers of specimens from specific materials, we can report that every specimen prepared here illustrated, as expected, ions with a uniform hit map, even during the very first experiments when attempting to fine-tune the alignment.

A second benefit of the in-situ protocol is enabling each specimen to come from a completely independent area to the others, i.e. not all linked on a single microcantilever. This can be beneficial, for example, when looking at the composition of grain boundaries, a topic of increasingly wide interest, such as in oxidation-induced segregation in aerospace Ni-superalloys [27,28], or radiation damage in nuclear RPV steels [29–31]. Genuine insights into grain boundaries require the ability to obtain statistically meaningful data across large numbers of these nanoscale interfaces. With conventional lift-out methods, the extracted material typically incorporates a single interface, but the shape of the boundary may be curved in three dimensions, reducing the chances of obtaining an interfacial region in each tip machined from a single (straight) lift-out. With an *in-situ* approach however, the user is free to machine individual tips wherever they choose in the microstructure. Locations could be selected to track a highly-curved interface, or selecting different grain boundaries within the same surface.

Conclusions

We have demonstrated the use of Xe-plasma FIB tools to directly machine viable APT samples in-situ, eliminating the need for lift-out procedures. The resulting specimens are robust, and their fabrication can be automated to run with minimal user input, and show negligible Xe-implantation. This simplified protocol offers significant benefits, particularly for the fabrication of APT materials that are prone to Ga-contamination within Ga FIB instruments.

Acknowledgements

The Glasgow Xe-plasma FIB is funded by the Engineering and Physical Sciences Research Council of the United Kingdom (EPSRC) under grant EP/P001483/1 and some of the work outlined here was conducted under EPSRC grant EP/N017218/1. The Oxford Atom Probe facility is also EPSRC funded, by grant EP/M022803/1. We gratefully acknowledge Adam Pilchak (Air Force Research Laboratory, Wright Patterson) and Chris Collins (Imperial College London) for supplying the additional Ti-alloy materials used in Fig. 5.

References

[1] D.W. Saxey, J.M. Cairney, D. McGrouther, T. Honma, S.P. Ringer, Atom probe specimen fabrication methods using a dual FIB/SEM, Ultramicroscopy 107 (2007) 756–760, https://doi.org/10.1016/j.ultramic.2007.02.024.

[2] K. Thompson, D. Lawrence, D.J. Larson, J.D. Olson, T.F. Kelly, B. Gorman, In situ site-specific specimen preparation for atom probe tomography, Ultramicroscopy 107 (2007) 131–139, https://doi.org/10.1016/j.ultramic.2006.06.008.

[3] K. Babinsky, W. Knabl, A. Lorich, R. De Kloe, H. Clemens, S. Primig, Grain boundary study of technically pure molybdenum by combining APT and TKD, Ultramicroscopy 159 (2015) 445–451, https://doi.org/10.1016/j.ultramic.2015.05.014.

[4] R. Ding, I.P. Jones, In situ hydride formation in titanium during focused ion milling, J. Electron Microsc. (Tokyo). 60 (2010) 1–9, https://doi.org/10.1093/jmicro/dfq066.

[5] A. Basa, C. Thaulow, A. Barnoush, Chemically induced phase transformation in austenite by focused ion beam, Metall. Mater. Trans. A. 45 (2014) 1189–1198, https://doi.org/10.1007/s11661-013-2101-4.

[6] R.P. Babu, S. Irukuvarghula, A. Harte, M. Preuss, Nature of gallium focused ion beam induced phase transformation in 316L austenitic stainless steel, Acta Mater 120 (2016) 391–402, https://doi.org/10.1016/J.ACTAMAT.2016.08.008.

[7] A.K. Revelly, G. Monpara, I. Samajdar, K.V.M. Krishna, R. Tewari, D. Srivastava, G.K. Dey, A.S. Panwar, Effect of gallium ion damage on poly-crystalline zirconium: direct experimental observations and molecular dynamics simulations, J. Nucl. Mater. 467 (2015) 155–164, https://doi.org/10.1016/J.JNUCMAT.2015.07.018.

[8] S. Rubanov, P.R. Munroe, Damage in III–V compounds during focused ion beam milling, Microsc. Microanal. 11 (2005) 446–455, https://doi.org/10.1017/S1431927605050294.

[9] F. Tang, M.P. Moody, T.L. Martin, P.A.J. Bagot, M.J. Kappers, R.A. Oliver, Practical issues for atom probe tomography analysis of iii-nitride semiconductor materials, Microsc. Microanal. 21, 03 21 (2015) 21, https://doi.org/10.1017/S1431927615000422.

[10] J. Bogdanowicz, A. Kumar, C. Fleischmann, M. Gilbert, J. Houard, A. Vella, W. Vandervorst, Laser-assisted atom probe tomography of semiconductors: the impact of the focused-ion beam specimen preparation, Ultramicroscopy 188 (2018) 19–23, https://doi.org/10.1016/j.ultramic.2018.03.001.

[11] K.A. Unocic, M.J. Daehn, G.S. Mills, Effect of gallium focused ion beam milling on preparation of aluminium thin foils, J. Microsc. 240 (2010) 227–238, https://doi.org/10.1111/j.1365-2818.2010.03401.x.

[12] M.K. Miller, A. Cerezo, M.G. Hetherington, G.D.W. Smith, Atom Probe Field Ion Microscopy, Oxford University Press, 1996.

[13] B. Gault, M.P. Moody, J.M. Cairney, S.P. Ringer, Atom Probe Microscopy, Springer, 2012.

[14] M.K. Miller, K.F. Russell, G.B. Thompson, Strategies for fabricating atom probe specimens with a dual beam FIB, Ultramicroscopy 102 (2005) 287–298, https://doi.org/10.1016/j.ultramic.2004.10.011.

[15] P. Felfer, I. McCarroll, C. Macauley, J.M. Cairney, A simple approach to atom probe sample preparation by using shadow masks, Ultramicroscopy 160 (2016) 163–167, https://doi.org/10.1016/j.ultramic.2015.09.005.

[16] T. Vermeij, E. Plancher, C.C. Tasan, Preventing damage and redeposition during focused ion beam milling: the “umbrella” method, Ultramicroscopy 186 (2018) 35–41, https://doi.org/10.1016/j.ultramic.2017.12.012.

[17] R. Estivill, G. Audoit, J.-P. Barnes, A. Grenier, D. Blavette, Preparation and analysis of atom probe tips by xenon focused ion beam milling, Microsc. Microanal. 22 (2016) 576–582, https://doi.org/10.1017/S1431927616000581.

[18] R.D. Kelley, K. Song, B. Van Leer, D. Wall, L. Kwakman, Xe+ FIB milling and measurement of amorphous silicon damage, Microsc. Microanal. 19 (2013) 862–863, https://doi.org/10.1017/S1431927613006302.

[19] T. Li, D. Kent, G. Sha, J.M. Cairney, M.S. Dargusch, The role of ω in the precipitation of α in near-β Ti alloys, Scr. Mater. 117 (2016) 92–95, https://doi.org/10.1016/j.scriptamat.2016.02.026.

[20] H.L. Wang, Y.L. Hao, S.Y. He, T. Li, J.M. Cairney, Y.D. Wang, Y. Wang, E.G. Obbard, F. Prima, K. Du, S.J. Li, R. Yang, Elastically confined martensitic transformation at the nano-scale in a multifunctional titanium alloy, Acta Mater. 135 (2017) 330–339, https://doi.org/10.1016/J.ACTAMAT.2017.06.040.

[21] A. Devaraj, S. Nag, R. Banerjee, Alpha phase precipitation from phase-separated beta phase in a model Ti–Mo–Al alloy studied by direct coupling of transmission electron microscopy and atom probe tomography, Scr. Mater. 69 (2013) 513–516, https://doi.org/10.1016/J.SCRIPTAMAT.2013.06.011.

[22] A. Radecka, J. Coakley, V.A. Vorontsov, T.L. Martin, P.A.J. Bagot, M.P. Moody, D. Rugg, D. Dye, Precipitation of the ordered α2 phase in a near-α titanium alloy, Scr. Mater. 117 (2016) 81–85, https://doi.org/10.1016/j.scriptamat.2016.02.015.

[23] D. Rugg, T.B. Britton, J. Gong, A.J. Wilkinson, P.A.J. Bagot, In-service materials support for safety critical applications – A case study of a high strength Ti- alloy using advanced experimental and modelling techniques, Mater. Sci. Eng. A. 599 (2014) 166–173, https://doi.org/10.1016/j.msea.2014.01.031.

[24] P.A.J. Bagot, A. Radecka, A.P. Magyar, Y. Gong, D.C. Bell, G.D.W. Smith, M.P. Moody, D. Dye, D. Rugg, The effect of oxidation on the subsurface microstructure of a Ti-6Al-4V alloy, Scr. Mater. 148 (2018) 24–28, https://doi.org/10.1016/j.scriptamat.2018.01.015.

[25] S. Subramaniam, J. Huening, J. Richards, K. Johnson, A comprehensive approach towards optimizing the xenon plasma focused ion beam instrument for semiconductor failure analysis applications, Microsc. Microanal. 23 (2017) 769–781, https://doi.org/10.1017/S1431927617000563.

[26] D. Cooper, J.-M. Hartmann, N. Gambacorti, Low energy Xe milling for the quantitative profiling of active dopants by off-axis electron holography, J. Appl. Phys. 110 (2011) 044511, , https://doi.org/10.1063/1.3625262.

[27] M.K. Miller, Contributions of atom probe tomography to the understanding of nickel-based superalloys, Micron 32 (2008) 757–764, https://doi.org/10.1016/S0968-4328(00)00083-4.

[28] S. Pedrazzini, D.J. Child, T. Aarholt, C. Ball, M. Dowd, A. Girling, H. Cockings, K. Perkins, M.C. Hardy, H.J. Stone, P.A.J. Bagot, On the effect of environmental exposure on dwell fatigue performance of a fine-grained nickel-based superalloy, Metall. Mater. Trans. A Phys. Metall. Mater. Sci. 49 , 9 (2018) 1–15, https://doi.org/10.1007/s11661-018-4752-7.

[29] C.A. Williams, E.A. Marquis, A. Cerezo, G.D.W. Smith, Nanoscale characterisation of ODS–Eurofer 97 steel: an atom-probe tomography study, J. Nucl. Mater. 400 (2010) 37–45, https://doi.org/10.1016/J.JNUCMAT.2010.02.007.

[30] N.A. Bailey, E. Stergar, M. Toloczko, P. Hosemann, Atom probe tomography analysis of high dose MA957 at selected irradiation temperatures, J. Nucl. Mater. 459 (2015) 225–234, https://doi.org/10.1016/J.JNUCMAT.2015.01.006.

[31] C.M. Barr, P.J. Felfer, J.I. Cole, M.L. Taheri, Observation of oscillatory radiation induced segregation profiles at grain boundaries in neutron irradiated 316 stainless steel using atom probe tomography, J. Nucl. Mater. 504 (2018) 181–190, https://doi.org/10.1016/J.JNUCMAT.2018.01.053.